

Effects of pluronic silica nanoparticles on the photophysical and photodynamic therapy behavior of triphenyl-p-phenoxy benzoic acid metalloporphyrins

Muthumuni Managa, Jonathan Britton, Earl Prinsloo & Tebello Nyokong

To cite this article: Muthumuni Managa, Jonathan Britton, Earl Prinsloo & Tebello Nyokong (2016) Effects of pluronic silica nanoparticles on the photophysical and photodynamic therapy behavior of triphenyl-p-phenoxy benzoic acid metalloporphyrins, Journal of Coordination Chemistry, 69:23, 3491-3506, DOI: [10.1080/00958972.2016.1236372](https://doi.org/10.1080/00958972.2016.1236372)

To link to this article: <https://doi.org/10.1080/00958972.2016.1236372>



Published online: 30 Sep 2016.



Submit your article to this journal [↗](#)



Article views: 286



View related articles [↗](#)



View Crossmark data [↗](#)



Citing articles: 4 View citing articles [↗](#)

Effects of pluronic silica nanoparticles on the photophysical and photodynamic therapy behavior of triphenyl-p-phenoxy benzoic acid metalloporphyrins

Muthumuni Managa^a, Jonathan Britton^a, Earl Prinsloo^b and Tebello Nyokong^a

^aDepartment of Chemistry, Rhodes University, Grahamstown, South Africa; ^bBiotechnology Innovation Centre, Rhodes University, Grahamstown, South Africa

ABSTRACT

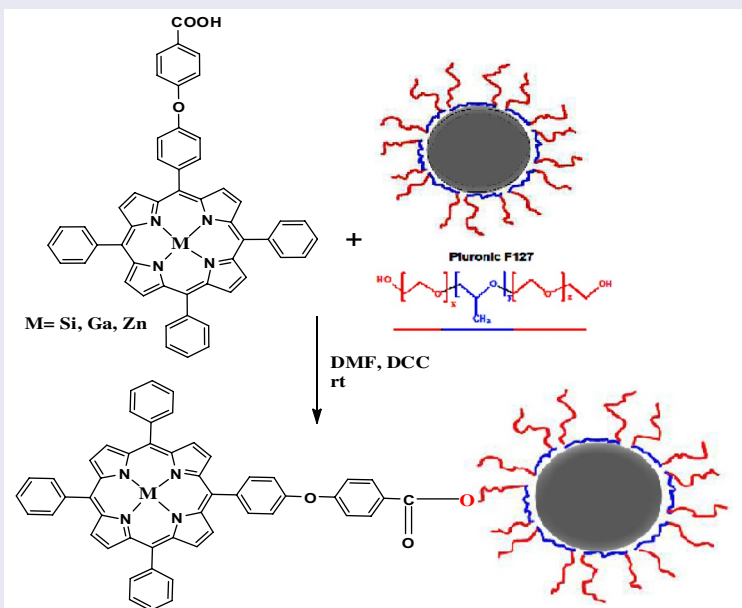
5, 10, 15, Triphenyl-20-p-phenoxy benzoic acid porphyrins (**P**) containing Zn (ZnP), Ga (GaP), and Si (SiP) were synthesized and conjugated to pluronic-silica (PluS) nanoparticles (NPs) where the fluorescence and singlet oxygen generating behavior of the porphyrins were investigated. The highest singlet oxygen quantum yield (Φ_{Δ}) was obtained for ZnP. When the porphyrins were conjugated to the PluS NPs, the Φ_{Δ} was quenched and fluorescence was enhanced. The pore size of the NPs upon conjugation decreased from 18.9 nm for PluS NPs to 2.4 nm (for ZnP as an example) as determined by applying the Brunauer–Emmett–Teller method. The porphyrin complexes and their conjugates were tested for their photodynamic therapy (PDT) activity on MCF-7 breast cancer cells. It was found that ZnP and its conjugate showed the highest PDT activity. The $p > 0.05$ indicated that ZnP is significantly different than GaP and SiP.

ARTICLE HISTORY

Received 11 June 2016
Accepted 23 August 2016

KEYWORDS

Porphyrin; pluronic silica nanoparticles; singlet oxygen quantum yield; photodynamic therapy



1. Introduction

Photodynamic therapy (PDT) is a minimally invasive treatment modality of tumor cells, which requires laser light of appropriate wavelength, a viable photosensitizer, and molecular oxygen [1, 2]. The electronically excited photosensitizer transfers its energy to ground state molecular oxygen to produce excited singlet oxygen, which acts as the chief cytotoxic species and thus, results in irreversible photo-damage of the tumor cells [1, 2]. Porphyrins are well-known photosensitizers for PDT [1]. Porphyrins containing carboxy groups are in clinical trials [2] hence carboxy porphyrins are employed in this work.

The interest in mesostructured silica nanomaterials has increased because of possible applications in the pharmaceutical and chemical industries [3]. *Meso* structured materials can be described as having pore sizes that range from 2 to 50 nm. When these materials are synthesized, the surfactant which is used is very important as it will influence the pore size. Silica-based nanoparticles (SiNPs) can be functionalized to allow for covalent and non-covalent immobilization of other molecules such as porphyrins.

In this work, pluronic 127 which is a non-ionic block copolymer was used for the synthesis of pluronic-silica nanoparticles (PluS NPs). Pluronic F127 is a poly(ethylene oxide)–poly(propylene oxide)–poly(ethylene oxide) (PEO–PPO–PEO) copolymer which forms micelles with the terminal PEO segment acting as a hydrophilic corona and PPO as a hydrophobic core [4]. The advantage of using pluronic 127 for the synthesis of NPs is that the pore size can be regulated using different temperatures [4]. It has been reported that the higher the temperature used for synthesis, the larger the pore size [4]. PluS NPs have low toxicity, show photophysical inertness, have high surface-to-volume ratio, and good water solubility [5]. Because of these properties, PluS NPs are compatible with most formulations for medical applications [6].

The porphyrins in this work are asymmetrically substituted to allow for a more defined linking to PluS NPs. This work reports on the linking of three porphyrin complexes (containing Zn, Ga and Si as central metals) separately to PluS NPs. The photophysical properties of the porphyrins are assessed when alone or when linked to PluS NPs. Porphyrins have been encapsulated into mesoporous SiNPs for drug delivery [6, 7], PDT [8], and for fluorescence sensing [9]. Porphyrins have also been covalently grafted onto mesoporous SiNPs [10]. The formation of nanoparticle–pluronic–porphyrin conjugate where pluronic moiety (not as nanoparticles) acts as a bridge has been reported [11]. This work reports a more controlled grafting of porphyrins onto PluS NPs and their PDT properties. Thus, the pluronic nanoparticles are chemically linked to porphyrins instead of the non-particle moiety used in the literature [11]. Nanoparticles are preferred due to increased surface area.

Pluronic F127 contains hydroxy end groups [12], and the porphyrins in this work contain a COOH allowing for linking to OH of PluS to form an ester bond. Si, Ga, and Zn were chosen as central metals due to their diamagnetic nature which together with the heavy metal effect of Ga and Zn will encourage intersystem crossing to the triplet state, ultimately improving singlet oxygen generation. As stated above, singlet oxygen is the cytotoxic species for PDT.

Symmetrically substituted porphyrins with carboxy phenoxy groups are known [13, 14]; however, the mono substituted derivative of this porphyrin is reported in this work for the first time. There are no reports in the literature on the Zn, Ga, and Si derivatives of this P, hence reported for the first time in this study. Their conjugation to PluS NPs, photophysical, and PDT studies is also reported for the first time.

2. Experimental

2.1. Materials

Pluronic 127 (MW ~12,600), pyrrole, tetraethyl orthosilicate (TEOS), 4-(4-formylphenoxy) benzaldehyde, dimethylformamide (DMF), dichloromethane (DCM), petroleum ether, dimethyl sulfoxide (DMSO), N,N dicyclohexylcarbodiimide (DCC), benzaldehyde, silicon tetrachloride, sodium azide, zinc chloride, gallium chloride, Zn tetraphenyl porphyrin (ZnTPP), and propionic acid were purchased from Sigma-Aldrich. The purification processes were carried out on silica gel 60 (0.063–0.200 mm) for column chromatography which was bought from Macherey-Nagel (MN) Germany. Cultures of MCF-7 breast cancer cell lines

were obtained from Cellonex®. Dulbecco's phosphate-buffered saline (DPBS), trypsin, ethylenediamine-tetraacetic acid, and Dulbecco's modified Eagle's medium (DMEM) were obtained from Lonza®, 10% (v/v) heat-inactivated fetal calf serum (FCS), neutral red cell proliferation reagent (WST), and 100 unit mL⁻¹ penicillin-100 µg mL⁻¹ streptomycin-amphotericin B were obtained from Biowest®.

2.2. Equipment

Ground state electronic absorption spectra were recorded at room temperature using a Shimadzu UV-2550 spectrophotometer and a 1-cm pathlength cuvette. Transmission electron microscope (TEM) images were obtained using a Carl Zeiss Libra transmission electron microscope operating at 100 kV accelerating voltage. Energy dispersive X-ray spectroscopy was carried out using a INCA PENTA FET coupled to the VAGA TESCAM using 20 kV accelerating voltage.

X-ray powder diffraction (XRD) patterns were recorded on a Bruker D8 Discover equipped with a Lynx Eye Detector, using Cu-K α radiation ($\lambda = 1.5405 \text{ \AA}$, nickel filter). Data were collected from $2\theta = 10\text{--}60^\circ$ scanning at 10 min^{-1} with a filter time constant of 2.5 s per step and a slit width of 6.0 mm. Samples were placed on a zero background silicon wafer slide. XRD data were treated using Eva (evaluation curve fitting) software. Baseline correction was performed on each diffraction pattern by subtracting a spline fitted to the curved background.

IR spectra were recorded on a Perkin-Elmer Spectrum 100 ATR FT-IR spectrometer. Fluorescence emission spectra were recorded on a Varian Eclipse spectrofluorometer. Elemental analyses were carried out on a Vario EL III MicroCube CHNS Analyzer. Mass spectral data were collected with a Bruker AutoFLEX III Smartbeam TOF/TOF Mass spectrometer. Details have been provided before [15]. ¹H NMR spectra were obtained using a Bruker AVANCE 600 MHz NMR spectrometer in CDCl₃-d₆.

The singlet oxygen generation was quantified using an ultrasensitive Germanium detector (Edinburgh Instruments, EI-P) combined with a 1000 nm long pass filter (Omega, 3RD 1000 CP) and a 1270 nm band pass filter (Omega, C1275, BP50) to detect the intensity of the singlet oxygen phosphorescence band at 1270 nm. These studies were done for all the porphyrins and their conjugates in DMF, in the absence and presence of sodium azide (a physical quencher of singlet oxygen). Details have been provided before [16].

Nitrogen adsorption/desorption isotherms were carried out at 77 K using a Micrometrics ASAP 2020 Surface Area and Porosity Analyzer. Prior to each measurement, degasing was carried out at 900 °C for four days. The Brunauer-Emmett-Teller (BET) method was employed to determine surface area and porosity. The BET surface area and total pore volume were calculated from the isotherms obtained. The details of the setup have been previously described [17].

Time-of-Flight Secondary Ion Mass Spectrometer (TOF-SIMS) data were recorded with ION TOF GmbH TOF SIMS 5-100 run in micro-raster mode. The raster area was 3000 µm × 3000 µm, and the sample was run in both positive and negative ion modes. The analyzer was set to a standard operating mode with a cycle time of 100 µs, while the primary beam was a Bi₃ ion cluster gun with a current of 0.4 pA and an energy of 3000 eV (also termed as spectrometry mode). The Bi₃ cluster and electron flood gun were used to get a better ion signal from the sample. Charge compensation was used to account for the electron flood gun. The raw data were processed using the SurfaceLab 6.5 software provided by ION TOF.

2.3. Synthesis

2.3.1. Synthesis of Pluronic Silica nanoparticles

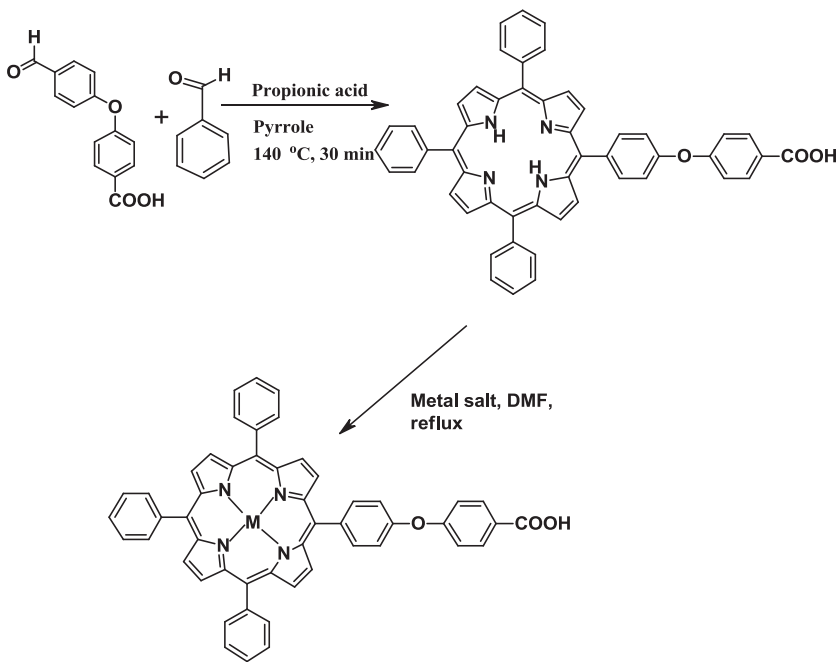
The nanoparticles were synthesized according to the literature [18] with slight modification as follows: Pluronic 127 (2 g) was dissolved in a mixture of H₂O (15 mL) and 2 M HCl (60 mL) and then TEOS (4.25 g) was added and the mixture was vigorously stirred at 45 °C for 20 h. The mixture was then further heated to 100 °C in an oven for 12 h and then cooled to room temperature. The resulting product was filtered and vacuum dried at room temperature. The product was then calcinated at 550 °C for 12 h.

2.3.2. Synthesis of porphyrins

2.3.2.1. Synthesis of 5, 10, 15, triphenyl-20-p-phenoxy benzoic acid porphyrin (H_2P), scheme 1. The synthesis was carried out with modification of the reported procedure [19, 20]. Benzaldehyde (3.98 g, 0.024 mol) and 4-(4-formylphenoxy) benzaldehyde (1.8 g, 0.0074 mol) were dissolved in 250 mL propionic acid and refluxed at 140 °C while vigorously stirring. Then, pyrrole (3.25 mL, 0.047 mol) was added dropwise through a dropping funnel. This mixture was refluxed for 30 min and allowed to cool to room temperature overnight. Methanol was then added and the solid left to precipitate, followed by filtration. Column chromatography using silica gel was carried out to purify the product using petroleum ether and DCM (1 : 3) as mobile phases, to give a dark purple product.

Yield: (72%). IR (KBr, cm^{-1}): 3278 (O–H), 1531 (C=C), 1374 (CH₂), 1006 (C–O), 770 (C–H). ¹H NMR 600 MHz, CDCl₃ δ (ppm) 8.86–8.81 (m, 6H) 8.23 (d, $J = 12$, 6H) 8.11 (d, $J = 6$, 2H) 7.81–7.74 (m, 17H) 7.24 (d, $J = 12$, 2H). UV/Vis (DMF) λ_{max} nm (log ϵ): 416 (4.99), 512 (4.27), 548 (3.89), 643 (3.22). Calcd for C₅₁H₃₄N₄O₃·H₂O = 79.96, H = 4.55, N = 7.28, Found: C = 80.52, H = 4.41 N = 7.21 MALDI-TOF-MS m/z Calcd: 750.84. Found (M–2H)⁺ 748.40

2.3.2.2. Synthesis of ClGa, Cl₂Si and Zn 5, 10, 15, triphenyl-20-p-phenoxy benzoic acid porphyrin (GaP, SiP and ZnP), scheme 1. The synthesis is as follows: DMF was brought to reflux in a two-necked flask while stirring and then metal free porphyrin synthesized above (3 g, 3.9 mmol) was added and temperature brought to 100 °C. Then, gallium chloride (1 g, 5.6 mmol), silicon tetrachloride (1.48 g, 8.7 mmol), or zinc chloride (1 g, 7.3 mmol) were added and heating continued for 15 min. The completion of the reaction was checked using a UV/Vis spectrophotometer. The reaction vessel was then allowed to cool in ice water. Ice cold water (500 mL) was added onto the resulting partially crystalline precipitate, which was then filtered, washed with water, and air dried. The product was purified by silica column chromatography. The color of SiP was dark green, while ZnP and GaP were plum/eggplant in color.



Scheme 1. Synthetic pathway of metal free, ClGa, Cl₂Si, and 5, 10, 15, triphenyl-20-p-phenoxy benzoic acid porphyrin, represented as GaP, SiP and ZnP.

GaP: Yield: (48%). IR (KBr, cm^{-1}): 3306 (O–H), 1556 (C=C), 1343 (CH_2), 962 (C–O), 791 (C–H). $^1\text{H NMR}$ (600 MHz, CDCl_3) δ (ppm): 8.91–8.86 (m, 4H), 8.23 (d, $J = 12$, 6H), 8.10 (d, $J = 6$, 2H), 7.82–7.76 (m, 17H), 7.24 (d, $J = 12$, 2H). UV/Vis (DMF) λ_{max} nm (log ϵ): 425 (4.23), 552 (3.87), 591 (3.35). Calcd for $\text{C}_{51}\text{H}_{32}\text{N}_4\text{O}_3\text{GaCl}\cdot\text{H}_2\text{O}$: C = 70.17, H = 3.78, N = 6.42, Found: C = 70.59, H = 3.68, N = 6.47 MALDI-TOF-MS m/z Calcd: 854.12. Found $(\text{M}-2\text{H})^+$ 852.23.

SiP: Yield: (52%). IR (KBr, cm^{-1}): 3306 (O–H), 1556 (C=C), 1343 (CH_2), 962 (C–O), 791 (C–H). $^1\text{H NMR}$ (600 MHz, CDCl_3) δ (ppm): 8.90–8.86 (m, 4H), 8.24 (d, $J = 12$, 6H), 8.10 (d, $J = 6$, 2H), 7.81–7.76 (m, 17H), 7.24 (d, $J = 12$, 2H). UV/Vis (DMF) λ_{max} nm (log ϵ): 446 (4.33), 662 (3.75) Calcd for $\text{C}_{51}\text{H}_{32}\text{N}_4\text{O}_3\text{SiCl}_2$: C = 72.25, H = 3.80, N = 6.61, Found: C = 72.16, H = 3.56, N = 6.24. MALDI-TOF-MS m/z Calcd: 846.16. Found $(\text{M}-\text{Cl})^+$ 812.36

ZnP: Yield: (67%). IR (KBr, cm^{-1}): 3306 (O–H), 1556 (C=C), 1343 (CH_2), 962 (C–O), 791 (C–H). $^1\text{H NMR}$ (600 MHz, CDCl_3) δ (ppm): 8.86 (m, 4H), 8.24 (d, $J = 12$, 6H), 8.10 (d, $J = 6$, 2H), 7.82–7.76 (m, 17H), 7.24 (d, $J = 12$, 2H). UV/Vis (DMF) λ_{max} nm (log ϵ): 429 (4.21), 559 (3.90), 599 (3.39). Calcd for $\text{C}_{51}\text{H}_{32}\text{N}_4\text{O}_3\text{Zn}\cdot 2\text{H}_2\text{O}$: C = 72.23, H = 3.95, N = 6.59, Found: C = 70.68, H = 3.42, N = 6.21 MALDI-TOF-MS m/z Calcd: 848.16. Found $(\text{M}-4\text{H})^+$ 844.23.

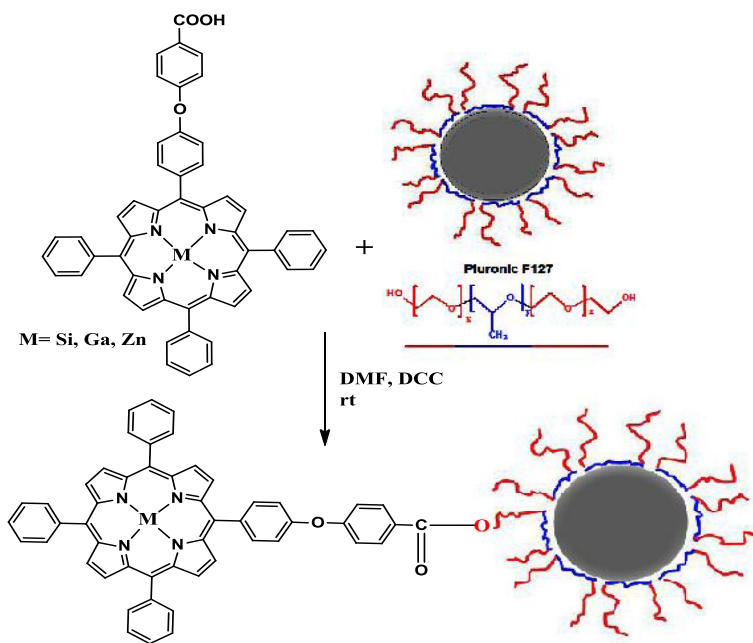
2.3.3. Conjugation of GaP, SiP, and ZnP to PluS NPs, to form GaP–PluS NPs, SiP–PluS NPs, and ZnP–PluS NPs, scheme 2

GaP, SiP, and ZnP (0.02 g, 0.023 to 0.025 mmol) were first dissolved in DMF (10 mL), then DCC (0.03 g, 0.145 mmol) was added to convert the carboxylic group (–COOH) of the porphyrin into an active carboxylate ester group. This mixture was stirred at room temperature for 24 h. After this time, 0.04 g of PluS NPs was added and the mixture stirred for further 24 h. The conjugate was separated from the un-conjugated nanoparticles using Bio-Beads S-X1 from Bio-Rad.

2.4. Cytotoxicity and PDT studies

2.4.1. In vitro dark cytotoxicity studies

MCF-7 carcinoma cells were cultured using DMEM containing 4.5 g L^{-1} glucose with L-glutamine (0.11 g L^{-1}) and phenol red, supplemented with 10% (v/v) heat-inactivated FCS (50 mL), and 100 unit mL^{-1}



Scheme 2. Covalent attachment of PluS NPs to the MP.

penicillin-100 $\mu\text{g mL}^{-1}$ streptomycin-amphotericin B. The cells were grown in 75 cm^2 vented flasks (Porvair®) and incubated at 37 °C and 5% CO_2 with humidified atmosphere. Once 90–100% cell confluence was achieved as determined through microscopic examination, the cells were rinsed with DPBS. The cells were passaged through routine trypsinization. Routine viability and cell enumeration were performed using the trypan blue dye exclusion assay (0.4% trypan blue solution) using a hemocytometer. Cells were seeded at a cell density of 10,000 cells/well in supplemented DMEM containing phenol red in 96-well tissue culture plates (Porvair®), and incubated in a humidified atmosphere at 37 °C and 5% CO_2 for 24 h to foster cell attachment to the wells. The attached cells were rinsed with 100 μL DPBS once, followed by administration of 100 μL supplemented DMEM containing gradient concentrations of 4.2×10^{-3} –0.06 mg mL^{-1} of PluS NPs, ZnP, GaP, and SiP and their conjugates. Vehicle controls were performed with fresh supplemented medium or medium containing comparable amounts of DMSO (0.1–0.8% (v/v)).

After 24-h incubation with supplemented DMEM with phenol red, cell proliferation neutral red reagent (WST-1) was used to quantify the surviving cells. The WST-1 assay was used to assess the toxicity and cell proliferation as per the manufacturer's instructions (Roche) using a Synergy 2 multi-mode microplate reader (BioTek®) at a wavelength of 450 nm.

The percent cell viability was determined using equation 1:

$$\% \text{ cell viability} = \frac{\text{Absorbance sample at 450 nm}}{\text{Absorbance control at 450 nm}} \times 100 \quad (1)$$

where the absorbance of sample is the cells containing ZnP, GaP, and SiP and their conjugates, while absorbance of control is the placebo cells containing only supplemented DMEM with phenol red.

2.4.2. PDT test

The PDT effects of the different complexes were investigated by incubating cells as explained above with varying concentrations of ZnP, GaP, and SiP and their conjugates with PluS NPs. The difference is that after incubation for 24 h and then washing with DPBS, the DMEM used did not contain phenol red. The photo-irradiations were performed using glass filtered light from a general electric quartz lamp (300 W) expanded to cover the plate, resulting in a power density of 93 mW cm^{-2} for each well. Water filter was then used to exclude any IR radiation. A quartz lamp has been reported to be an effective light source in the photo-irradiation of tumor cells [21]. The irradiation time was 300 s to result in irradiation doses of 28 J cm^{-2} . After irradiation, the medium was replaced with a fresh one containing phenol red. The absorbance of the cells was measured at an excitation wavelength of 450 nm using a Synergy 2 multi-mode microplate reader (BioTek1) discussed above. There were no changes in the spectra of the porphyrins following irradiation for PDT studies, hence confirming stability.

2.4.3. Statistical analysis

The data obtained from the three independent triplicate experiments were analyzed with a three-way factorial ANOVA (analysis of variance) to determine the statistical differences between the *in vitro* cytotoxicity and photodynamic effect of the photosensitizers on MCF-7 cancer cells. TukeyHSD *post hoc* test was used to determine the mean differences *in vitro* photodynamic effect of the photosensitizers on MCF-7 cancer cells. *p*-value of < 0.05 was considered significant.

3. Results and discussion

3.1. Characterization of SiP, GaP and ZnP

^1H NMR and IR spectroscopy, mass spectrometry as well as elemental analyses were employed for characterization of the porphyrins and gave satisfactory results. The C, H, and N elemental analysis data of complexes are in agreement with their structure, and are consistent with the fact that porphyrins are often isolated as solvates [22].

Porphyrins are characterized by an intense band called the Soret or B band at about 400 nm. The Q bands are observed between 500 and 600 nm. Figure 1 shows the spectra of ZnP, GaP, and SiP. The Soret band of ZnP is at 427 nm, while the Q bands are at 563 and 604 nm. The Soret bands of GaP and SiP are observed at 425 and 446 nm, respectively, table 1. Thus, the Soret band of SiP is highly red-shifted compared to ZnP and GaP. Red-shift of Soret bands is often observed for distorted porphyrins [23]. The Q bands for GaP are observed at 551 and 590 nm. A very prominent and intense Q band is observed at 669 nm for SiP with a weaker second component, figure 1. Metallated porphyrins contain two Q bands called α (high energy band) and β (low energy band) [24]. The relative intensities of these bands have been associated with the stability of the metal complex. When $\alpha > \beta$ as is the case for GaP and ZnP, the metal forms a stable square-planar porphyrin complex [24]. For SiP $\beta > \alpha$, implying an unstable complex where the central metal can easily be displaced.

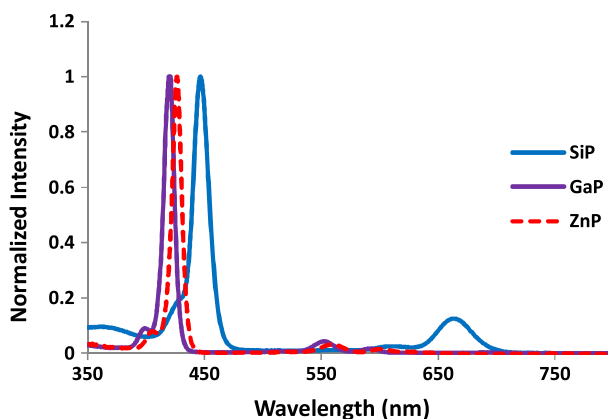


Figure 1. Absorption spectra of SiP (Blue), GaP (Purple) and ZnP (Red). Solvent = DMF.

Table 1. Fluorescence and singlet oxygen quantum yields of GaP, SiP and ZnP as well as GaP–PluS NPs, SiP–PluS NPs and ZnP–PluS NPs.

Complex	λ (Soret)/nm	$(\Phi_F)^a$	$(\Phi_\Delta)^a$
ZnP	427	0.09 (0.11)	0.41 (0.33)
GaP	425	0.12 (0.17)	0.38 (0.30)
SiP	446	0.15 (0.22)	0.35 (0.29)

^aValues in brackets are those of the conjugates.

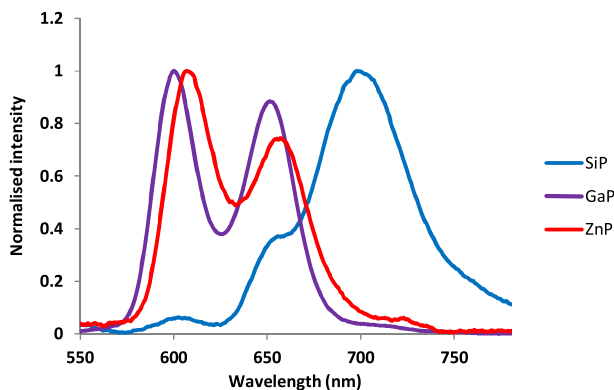


Figure 2. Fluorescence emission spectra of SiP (Blue), GaP (Purple) and ZnP (Red). Solvent = DMF.

Figure 2 shows the emission spectra of Zn and GaPs, which are typical [25] of a metallated porphyrin with two bands differing in intensity at 605 and 652 nm for ZnP, and 604 and 648 nm for GaP. However, SiP gave an emission which is not typical for metallated porphyrins, corresponding to the absorption spectra above.

3.2. Characterization of conjugates of PluS NPs with porphyrins

3.2.1. UV-vis spectra

Conjugation of PluS NPs to the porphyrin complexes is shown in scheme 2. There was no change in spectra following conjugation of the ZnP to PluS NPs, figure 3 (ZnP-PluS NPs was used as an example). The PluS NPs showed no absorption.

3.2.2. TEM and energy dispersive spectra

Figure 4A shows TEM images of PluS NPs. The particles are mono dispersed with an average size of 163 nm (see accompanied histogram, figure 4(B)). The PluS NPs particles are spherical. Upon conjugation

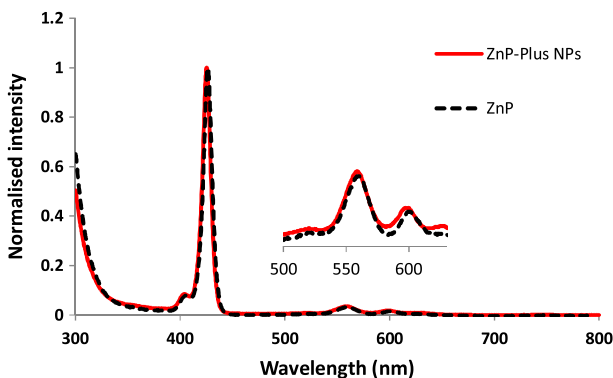


Figure 3. Absorption spectra of ZnP-PluS NPs.

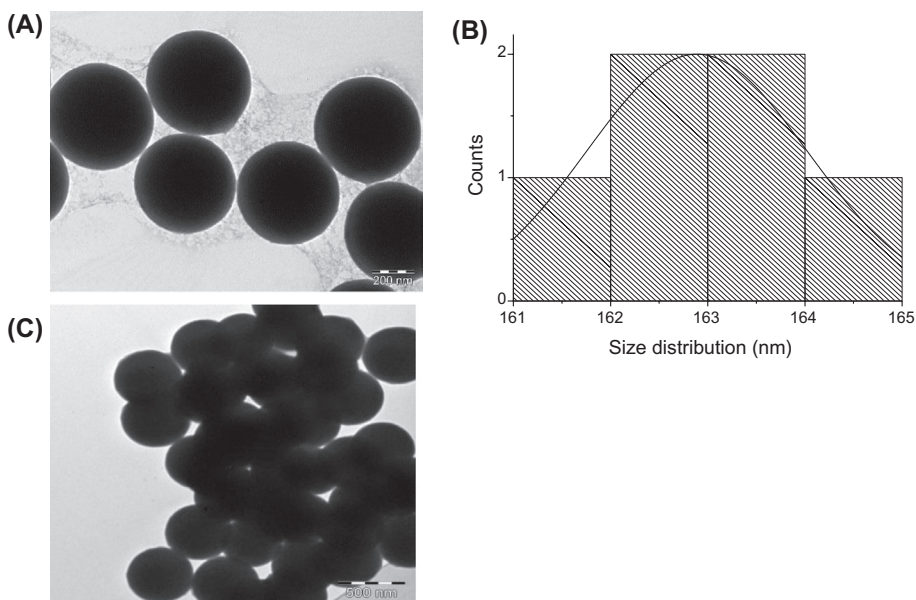


Figure 4. (A) TEM micrographs, accompanied histogram (B) of PluS NPs and (C) ZnP-PluS NPs conjugate as an example.

the PluS NPs to ZnP (as an example in figure 4(C)), aggregation was observed. It was difficult to obtain the overall average size for all the ZnP–PluS NPs due to aggregation. Energy dispersive spectra (EDS) were carried out to determine the elemental composition of the PluS NPs. Si and O (from the Si NPs core) were the major elements and carbon was observed from the pluronic 127 coating as shown in figure 5; no other peaks were observed rather than the reference peak 0 keV.

3.2.3. XRD

The XRD pattern for the PluS NPs, figure 6, shows a broadband between $2\theta = 20^\circ$ to 40° . The broadness of the band confirms the amorphous nature (as a result of the surfactant) of the nanoparticles. The amorphous nature continues following conjugation to porphyrins (figure 6). XRD was employed for crystalline size determination using figure 6 and the Debye Scherrer equation 2 [26]:

$$L = \frac{0.9\lambda}{\beta \cos\theta} \quad (2)$$

where k is an empirical constant equal to 0.9, λ is the wavelength of the X-ray source, (1.5405 \AA), β is the full width at half maximum of the diffraction peak, and θ is the angular position of the peak.

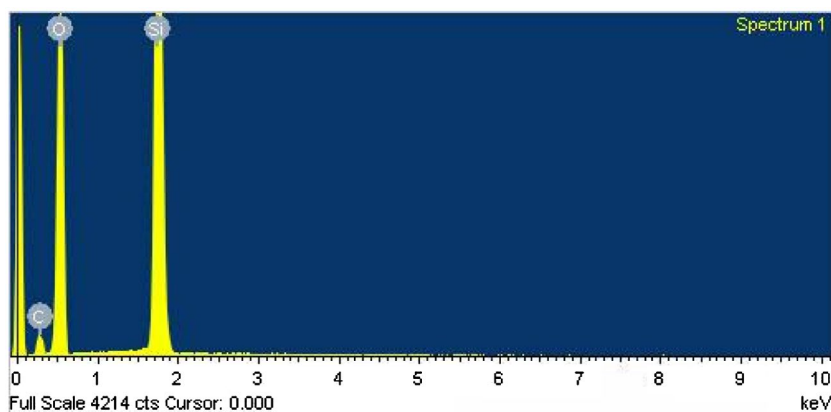


Figure 5. Energy dispersive spectra (EDS) of PluS NPs.

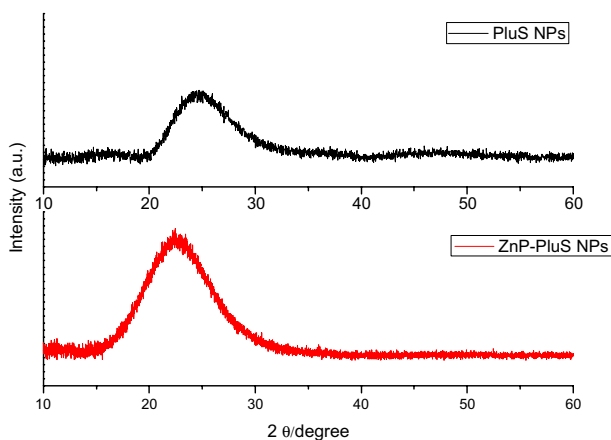


Figure 6. X-ray powder diffraction (XRD) of PluS NPs and ZnP–PluS NPs conjugate.

The average particle size was determined as 161 nm which is similar to that obtained by TEM. The size following conjugation does not change much due to the large size of the PluS NPs compared to the size of the porphyrins (~1 nm).

3.2.4. TOF-SIMS

The PluS NPs composition was further confirmed using TOF-SIMS, figure 7. TOF-SIMS is a very sensitive surface analytical technique. It provides detailed elemental and molecular information about surfaces, thin layers, interfaces, and full 3-D analysis of the samples. The mass distribution spectra (figure 7(B)) together with the images (figure 7(A)) showed the surface elemental compositions mostly to be -C,

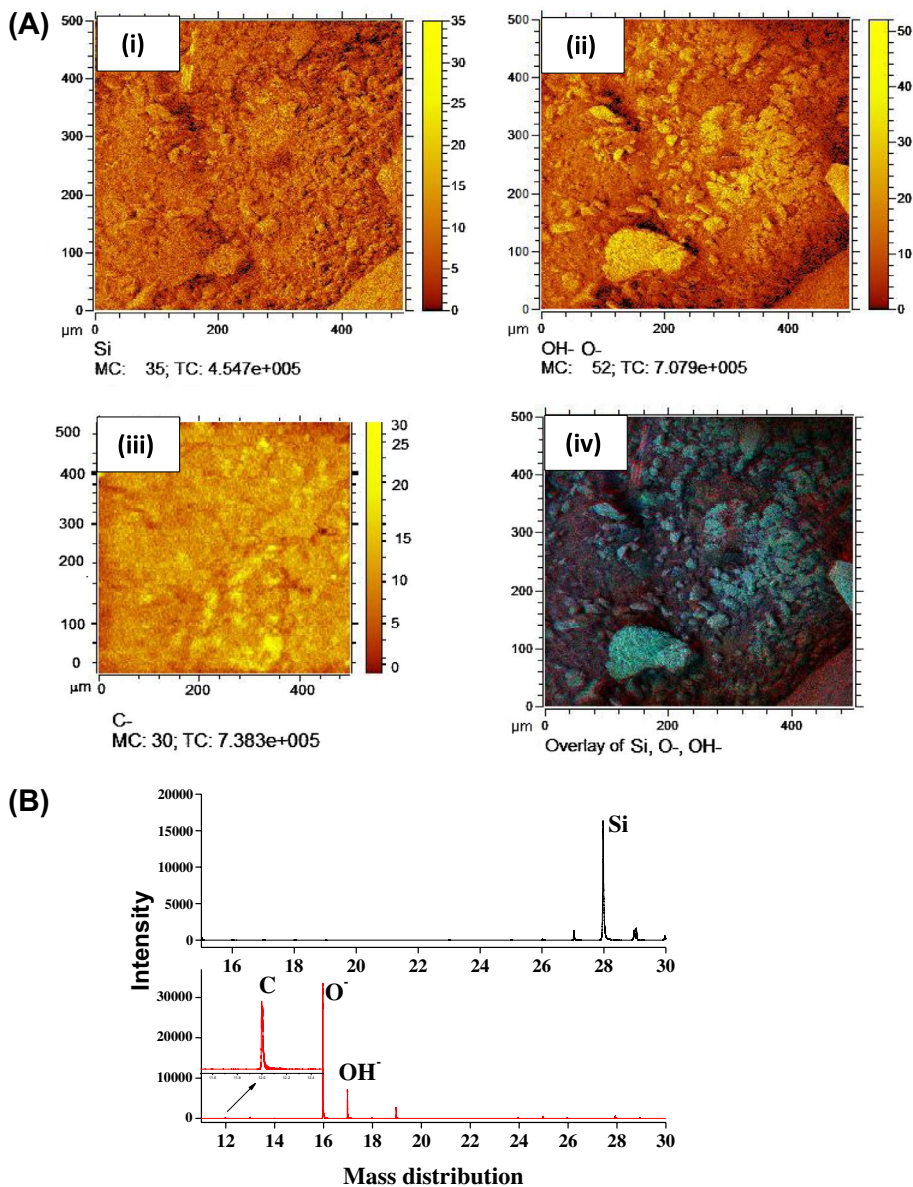


Figure 7. (A) TOF-SIMS images of (i) Si, (ii) OH⁻, O⁻, (iii) C and (iv) overlay of (i), (ii) and (iii) and (B) spectra of the mass distribution of PluS NPs.

–OH, O[−], and Si and further showed –OH both in the positive and negative mode. In figure 7(A), the side bar gives the concentration of the ions. figure 7(A)(i) shows a high concentration of Si from the silica core, figure 7(A)(ii) shows an even higher content of OH[−] and O[−] from Pluronic F127 which contains poly(ethylene oxide)–poly(propylene oxide)–poly(ethylene oxide) units as described above. Figure 7(A) (iii) shows the content from Pluronic F127.

3.2.5. BET

BET was performed to determine the pore size and surface area of the PluS NPs before and after linking to porphyrin. The pore size of the PluS NPs was determined to be 18.9 nm and the surface area was 330 m² g^{−1}. The isotherm describes the partitioning between gas phase and adsorbed species as a function of applied pressure. The isotherm of the nanoparticles was shown to be type 4 which also indicates the mesoporous nature of the nanoparticles (figure 8(A)). Type 4 BET isotherm indicates an indefinite multilayer formation after completion of the monolayer and is found in adsorbents with a wide distribution of pore sizes. The BET isotherm of ZnP–PluS NPs conjugate, figure 8(B), was used as an example as similar trends were observed for the other conjugates. Figure 8(B) shows that the isotherm for the ZnP–PluS NPs conjugate is type 1 which depicts monolayer adsorption. This suggests that the porphyrins prevent multilayer formation, hence type IV4 isotherm observed for PluS alone is not observed for the conjugate. The pore size decreased from 18.9 nm for PluS NPs to 2.4 nm for ZnP–PluS NPs conjugate. The surface area for the conjugate is 192.5 m² g^{−1}, a decrease from 330 m² g^{−1} for PluS NPs alone. Therefore, both pore size and surface area decreased for PluS NPs on conjugation to porphyrins. It has been documented that a rough surface results in larger surface area than a smooth one [27]. Thus, the observed decrease in surface area in the presence of the porphyrin suggests decreased roughness. The decrease in pore size in the presence of porphyrins may suggest that the porphyrins might have been entrapped in the pore of the PluS NPs, causing a reduction in the pore size.

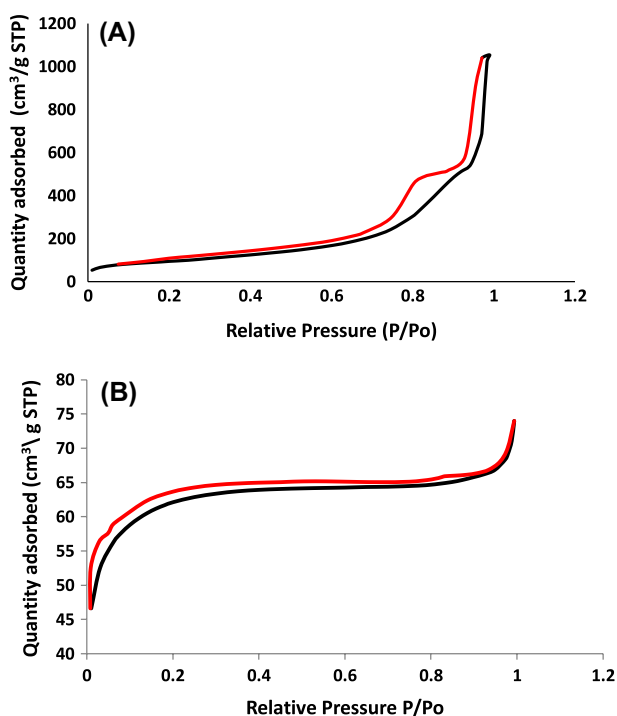


Figure 8. Nitrogen adsorption-desorption isotherm of (A) PluS NPs and (B) PluS linked to ZnP. The red line denotes the absorption while the black lines are desorption of the sample.

3.2.6. FTIR

The conjugation of the porphyrins to the PluS NPs using an ester bond was confirmed using FT-IR spectra. The ester bond can be observed at 1651 cm^{-1} figure 9 for ZnP–PluS NPs conjugate, confirming conjugation via an ester bond. Aliphatic C–H vibrations can be seen at 2929 cm^{-1} , while OH vibration is at 3473 cm^{-1} . The FT-IR of PluS NPs shows Si–O–Si peak at 1054 cm^{-1} , Si–O peak at 795 cm^{-1} , and the OH peak at 3340 cm^{-1} . The Si–O–Si peak and Si–O peak are within the range reported [28].

3.3. Photophysical studies

3.3.1. Fluorescence quantum yields (Φ_F)

Fluorescence quantum yields (Φ_F) were calculated using established comparative methods [29] and using ZnTPP as a standard ($\Phi_F^{\text{Std}} = 0.033$ [30]). Low Φ_F values of 0.09 to 0.15 were obtained for porphyrins alone. Even lower Φ_F values were obtained for GaP and ZnP (containing heavy central metals) due to the internal heavy atom effect which enhances intersystem crossing to the triplet state [31]. Generally, metalloporphyrins have low Φ_F as observed in this work and reported in literature [31]. There is a slight increase in fluorescence quantum yields of the porphyrin in the presence of PluS NPs, table 1. It has been reported [7] that embedding porphyrins in Pluronic NPs lead to the recovery of the fluorescence of the former. Thus, the increase in the fluorescence quantum yields of the porphyrin could be due to their protection by the PluS NPs.

3.3.2. Singlet oxygen quantum yield (Φ_{Δ})

As stated previously, singlet oxygen is the chief cytotoxic species responsible for cell death in PDT, hence its quantification is important. The time-resolved phosphorescence decay curve of singlet oxygen (figure 10) at 1270 nm was used to determine singlet oxygen quantum yield of GaP, SiP, and ZnP and their conjugates with PluS NPs in DMF using equation (3) [32]:

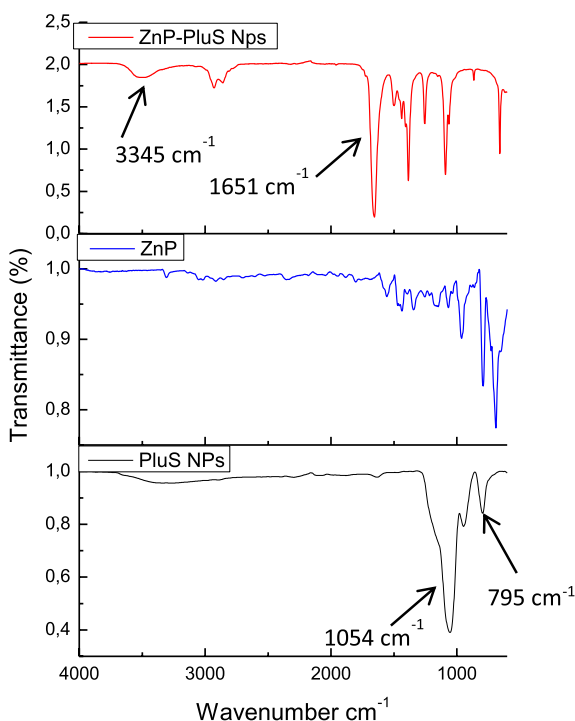


Figure 9. FTIR spectra of ZnP–PluS NPs conjugate (as an example), PluS NPs and ZnP alone.

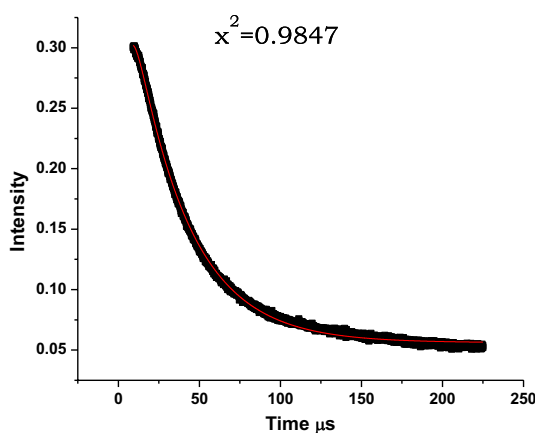


Figure 10. Singlet oxygen phosphorescence decay curve for ZnP-PluS NPs. Solvent = DMF.

$$I(t) = B \frac{\tau_D}{\tau_T - \tau_D} [e^{-t/\tau_T} - e^{-t/\tau_D}] \quad (3)$$

where $I(t)$ is the phosphorescence intensity of $^1\text{O}_2$ at time t , τ_D is the lifetime of $^1\text{O}_2$ phosphorescence decay, τ_T is the triplet state lifetime of the standard or sample, B is a coefficient involved in sensitizer concentration, and $^1\text{O}_2$ is the quantum yield. The singlet oxygen quantum yield, Φ_Δ of the complex was then determined in DMF, using equation (4):

$$\Phi_\Delta = \Phi_\Delta^{\text{Std}} \cdot \frac{B \cdot A^{\text{Std}}}{B^{\text{Std}} \cdot A} \quad (4)$$

where Φ_Δ^{Std} is the singlet oxygen quantum yield for the standard Zn tetraphenyl porphyrin (ZnTPP) $\Phi_\Delta^{\text{Std}} = 0.53$ in DMF [33], B and B^{Std} refer to coefficient involved in sensitizer concentration, and $^1\text{O}_2$ is the quantum yield for the sample and standard, respectively; A and A^{Std} refer to the absorbance of the sample and standard, respectively, at the excitation wavelength. The Φ_Δ was calculated to be 0.41 for ZnP and 0.33 for ZnP-PluS NPs conjugate, table 1. There was also a decrease in Φ_Δ values for GaP-PluS and SiP-PluS NPs conjugates compared to corresponding porphyrins alone. Such a decrease in Φ_Δ values could be explained by silica nanoparticles being singlet oxygen quenchers [34]. It has also been reported that inclusion of photosensitizers in nanocarriers results in less production of reactive oxygen species due to self-quenching of the excited states [35].

3.4. MCF-7 breast cancer cell studies

The stock concentrations of all complexes were prepared by dissolving them in DMSO and then making the volume up with supplemented media. We have reported before that 0.8% (v/v) DMSO had negligible effect on the cells [36], and this was also observed in this work.

3.4.1. In vitro dark cytotoxicity assay

The *in vitro* cytotoxicity of the porphyrins, PluS NPs, and their conjugates was evaluated against human breast cancer (MCF7) using WST-1 assay. PluS NPs alone are not toxic (figure 11(A)) and the $p > 0.05$ indicated that there is no significant difference within the concentrations.

The cytotoxicity of the porphyrin and the conjugates was low without light (dark toxicity), (figure 11(B)) (ZnP and its conjugate were used as examples) with all showing the cell viability above 80%. High percentage cell viability represents low dark toxicity.

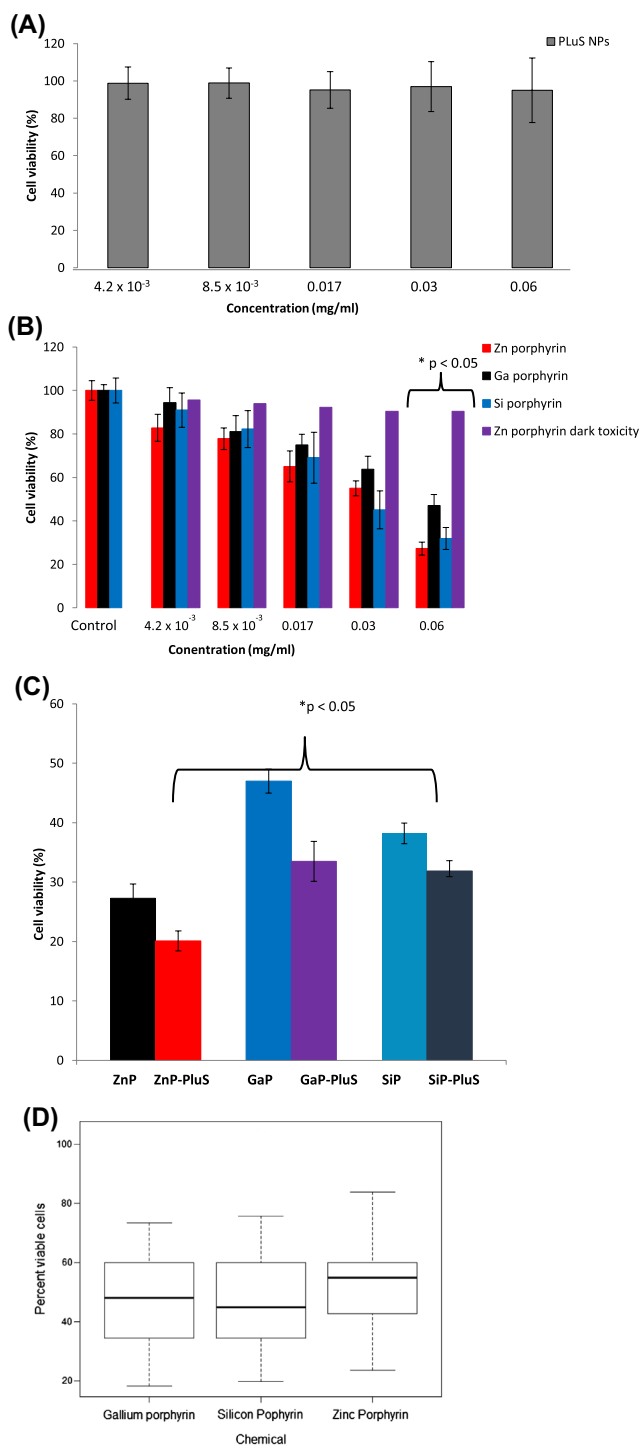


Figure 11. (A) dark toxicity plot of PluS NPs; (B) PDT activity of P alone; (C) comparison of PDT activities of the P and their conjugates at 0.06 mg mL⁻¹; (D) Distribution of the porphyrins –PluS NPs conjugates at 0.06 mg mL⁻¹. Statistically, there is significant difference between phototoxicity effects of ZnP and other porphyrin complexes as $p < 0.05$. Irradiation for 5 min for PDT activity and vehicle control was carried out.

3.4.2. PDT activities

The phototoxicity of porphyrin molecules increased upon irradiation and increased with increase in concentration, figure 11(B). ZnP (figure 11(B)) at 4.2×10^{-3} mg mL⁻¹ showed $83 \pm 4\%$ cell viability but at 0.06 mg mL⁻¹ there was a decrease to $27 \pm 3\%$. ZnP has the highest PDT effect followed by SiP and then GaP, figure 11(B). ZnP gave the largest singlet oxygen quantum yield of all the porphyrins (GaP and SiP), hence the increased PDT activity. As stated in the introduction, singlet oxygen is the cytotoxic species for PDT, hence the larger the singlet oxygen the better the PDT activity. It was observed that the percent cell viability decreased more for the conjugates of porphyrins with PluS NPs when compared to the porphyrins alone (compare figure 11(B) and 11(C)). The increase in PDT activity of the porphyrins in the presence of PluS NPs may be due the latter acting as the delivering agents and increasing solubility of the compounds. The highest PDT effect was achieved for ZnP–PluS NPs conjugate due to larger singlet oxygen quantum yields. ZnP conjugate at 0.06 mg mL⁻¹ showed $20 \pm 2\%$ cell viability, followed by GaP conjugate at $33 \pm 3\%$, and SiP conjugate at $38 \pm 4\%$ cell viability. The $p > 0.05$ indicated that ZnP is significantly different compared to the other porphyrins.

Figure 11(D) shows a box plot of ZnP, GaP, and SiP conjugates at 0.06 mg mL⁻¹; it is evident that phototoxicity is highest when ZnP is applied as evidenced by the higher distribution of the mean reflecting an over 70 percentile efficiency in PDT in comparison to GaP and SiP conjugates.

4. Conclusion

ClGa, Cl₂Si, and Zn 5, 10, 15, triphenyl-20-p-formylphenoxy acetic acid porphyrin were synthesized and conjugated to pluronic-silica nanoparticles (PluS NPs). Upon conjugation to PluS NPs, it was observed that the fluorescence quantum yield of the porphyrin complexes increased but singlet oxygen quantum yields decreased. These compounds and their conjugates were further tested for PDT activity on MCF-7 breast cancer cells. The PluS NPs improved the PDT activity of the porphyrins. The best activity was obtained for ZnP when alone or linked to PluS NPs.

Disclosure statement

No potential conflict of interest was reported by the authors.

Funding

This work was supported by the Department of Science and Technology (DST)/Nanotechnology (NIC) and National Research Foundation (NRF) of South Africa through DST/NRF South African Research Chairs Initiative for Professor of Medicinal Chemistry and Nanotechnology [garnt number UID62620] and Rhodes University.

References

- [1] R. Pandey, G. Zheng. In *The Porphyrin Handbook*, K.M. Kadish, K.M. Smith, R. Guilard (Eds), Vol. 6, Academic Press (2000).
- [2] R. Bonnett. In *Chemical Aspects of Photodynamic Therapy*, Gordon and Breach Science Publishers, Amsterdam (2000).
- [3] X. Hu, S. Spada, S. White, S. Hudson, E. Magner, J.G. Wall. *J. Phys. Chem.*, **110**, 18703 (2006).
- [4] D. Zhao, J. Feng, Q. Huo, N. Melosh, G.H. Fredrickson, B.F. Chmelka, G.D. Stucky. *Science*, **279**, 548 (1998).
- [5] S. Bonacchi, D. Genovese, R. Juris, M. Montalti, L. Prodi, E. Rampazzo, M. Sgarzi, N. Zaccheroni. *Top Curr. Chem.*, **300**, 93 (2011).
- [6] F. Figueira, J.A.S. Cavaleiro, J.P.C. Tomé. *J. Porphyr. Phthalocya.*, **15**, 517 (2011).
- [7] C. Mauriello-Jimenez, J. Croissant, M. Maynadier, X. Cattoën, M.W.C. Man, J. Vergnaud, V. Chaleix, V. Sol, M. Garcia, M. Gary-Bobo, L. Raehm, J.-O. Durand. *J. Mater. Chem. B*, **3**, 3681 (2015).
- [8] E. Secret, M. Maynadier, A. Gallud, A. Chaix, E. Bouffard, M. Gary-Bobo, N. Marcotte, O. Mongin, K. El Cheikh, V. Hugues, M. Auffan, C. Frochot, A. Morère, P. Maillard, M. Blanchard-Desce, M.J. Sailor, M. Garcia, J. Durand, F. Cunin. *Adv. Mater.*, **26**, 7643 (2014).
- [9] N. Masiera, J. Buczyńska, G. Orzanowska, H. Piwoński, J. Waluk. *Methods Appl. Fluoresc.*, **2**, 024003 (2014).
- [10] E. Secret, M. Maynadier, A. Gallud, M. Gary-Bobo, A. Chaix, E. Belamie, P. Maillard, M.J. Sailor, M. Garcia, J. Durand, F. Cunin. *Chem. Comm.*, **49**, 4202 (2013).

- [11] N. A. AksenoVA, V. V. Kardumyan, N. N. Glagolev, V. T. Shashkova, I. A. Matveeva, P. S. Timashev, and A. B. Solov'eva, *Russian J. Phys. Chem. A*, **89**, 1486 (2015).
- [12] W. Arap, R. Pasqualini, M. Montalti, L. Petrizza, L. Prodi, E. Rampazzo, N. Zaccheroni, S. Marchio. *Curr. Med. Chem.*, **20**, 2195 (2013).
- [13] E.-Y. Jeong, A. Burri, S.-Y. Lee, S.-E. Park. *J. Mater. Chem.*, **20**, 10869 (2010).
- [14] D. Vlascici, E. Fagadar-Cosma, I. Popa, V. Chiriac, M. Gil-Agusti. *Sensors*, **12**, 8193 (2012).
- [15] N. Masilela, T. Nyokong. *J. Photochem. Photobiol. A*, **223**, 124 (2011).
- [16] P. Modisha, E. Antunes, J. Mack, T. Nyokong. *Int. J. Nanosci.*, **12**, 1350010 (2013).
- [17] A. Fashina, E. Antunes, T. Nyokong. *Polyhedron*, **53**, 278 (2013).
- [18] B. Lee, Z. Ma, Z. Zhang, C. Park, S. Dai. *Microporous Mesoporous Materials*, **122**, 160 (2009).
- [19] A.D. Adler, F.R. Longo, J.D. Finarelli, J. Goldmacher, J. Assour, L. Korsakoff. *J. Org. Chem.*, **32**, 476 (1967).
- [20] E. Fagadar-Cosma, D. Vlascici, M. Birdeanu, G. Fagadar-Cosma, *Arabian J. Chem*, *In Press*
- [21] M. Alexiades-Armenakas. *Clin. Dermatol.*, **24**, 16 (2006).
- [22] I. Kos, L. Benov, I. Spasojević, J.S. Rebouças, I. Batinić-Haberle. *J Med Chem.*, **52**, 7868 (2009).
- [23] S.J. Takayama, G. Ukpabi, M.E.P. Murphy, A.G. Mauk. *PNAS*, **108**, 13071 (2011).
- [24] R. Giovannetti. In *Macro To Nano Spectroscopy*, J. Uddin (Ed.), Intech, Open science, Croatia, pp. 79–87 (2012).
- [25] M. Uttamlal, A.S. Holmes-Smith. *Chem. Phys. Lett.*, **454**, 223 (2008).
- [26] S. Sapra, D. Sarma. *Pramana – J. Phys.*, **65**, 565 (2005).
- [27] S. Xu, S. Hartvickson, J.X. Zhao, A.C.S. Appl. *ACS Appl. Mater. Interfaces*, **3**, 1865 (2011).
- [28] M.J.L. Portole's, F.R. Nieto, D.B. Soria, J.I. Amalvy, P.J. Peruzzo, D.O. Ma'rtire, M. Kotler, O. Holub, M.C. Gonzalez. *J. Phys. Chem. C*, **113**, 13702 (2009).
- [29] S. Fery-Forgues, D. Lavabre. *J. Chem. Educ.*, **76**, 1260 (1999).
- [30] R. L. Brookfield, H. Ellul, A. Harriman, G. Porter, *J. Chem. Soc., Faraday Trans.*, **82**, 219 (1986).
- [31] J.M. Dąbrowski, B. Pucelik, M.M. Pereira, L.G. Arnaut, G. Stochel. *J. Coord. Chem.*, **68**, 3116 (2015).
- [32] M.S. Patterson, S.J. Madsen, R. Wilson. *J. Photochem. Photobiol. B: Biol*, **5**, 69 (1990).
- [33] W. Spiller, H. Kliesch, D. Wöhrle, S. Hackbarth, B. Röder, G. Schnurpfeil. *J. Porphyr. Phthalocya*, **2**, 145 (1998).
- [34] C.R. Lillo, J. J. Romero, M. L. Portolés, R. P. Diez, P. C. Caregnato, M.C. Gonzalez, *Nano Res.* **8**, 2047 (2015).
- [35] N. Nishiyama, Y. Morimoto, W.-D. Jang, K. Kataoka. *Adv. Drug Deliv. Rev.*, **61**, 327 (2009).
- [36] R.O. Ogbodu, J.L. Limson, E. Prinsloo, T. Nyokong. *Synthetic Met.*, **204**, 122 (2015).